

Many-body electronic structure and Kondo properties of cobalt-porphyrin moleculesLuis G. G. V. Dias da Silva,^{1,2,*} Murilo L. Tiago,¹ Sergio E. Ulloa,³ Fernando A. Reboredo,¹ and Elbio Dagotto^{1,2}¹*Materials Science and Technology Division, Oak Ridge National Laboratory, Oak Ridge, Tennessee 37831, USA*²*Department of Physics and Astronomy, University of Tennessee, Knoxville, Tennessee 37996, USA*³*Department of Physics and Astronomy, Nanoscale and Quantum Phenomena Institute, Ohio University, Athens, Ohio 45701-2979, USA*

(Received 15 May 2009; revised manuscript received 18 September 2009; published 21 October 2009)

We use a combination of first-principles many-body methods and the numerical renormalization-group technique to study the Kondo regime of cobalt-porphyrin compounds adsorbed on a Cu(111) surface. We find the Kondo temperature to be highly sensitive to both molecule charging and distance to the surface, which can explain the variations observed in recent scanning-tunneling-spectroscopy measurements. We discuss the importance of many-body effects in the molecular electronic structure controlling this phenomenon and suggest scenarios where enhanced temperatures can be achieved in experiments.

DOI: [10.1103/PhysRevB.80.155443](https://doi.org/10.1103/PhysRevB.80.155443)

PACS number(s): 73.22.-f, 72.15.Qm, 71.10.-w, 71.15.-m

I. INTRODUCTION

Predicting the electronic properties of magnetic nanostructures is a challenging task as magnetism often manifests itself as a delicate interplay between spin-ordering surface chemistry and finite-size effects.^{1,2} Nanoscale magnetism is at the heart of several proposals for molecular spintronic devices, highlighting the need for a detailed understanding of spin-related phenomena in these systems. One important and especially subtle example of this behavior is the Kondo effect, arising from many-body spin interactions between a magnetic impurity and electrons in a metallic system.³

At low temperatures, the Kondo screening of the impurity's magnetic moment creates a sharp resonance at the Fermi energy in the local density of states at/near the magnetic impurity, producing a zero-bias anomalous signal in transport experiments that probe the local structure. Scanning-tunneling microscopy (STM) has proved to be an outstanding tool to probe signatures of the Kondo effect in magnetic adatoms on metallic surfaces.⁴⁻⁷ More recently, Kondo-type signals have been reported in magnetic molecules adsorbed on metallic substrates,⁸⁻¹² stimulating significant advances on the theory side.¹³⁻²¹ For both single magnetic atoms and magnetic molecules on metallic surfaces, the low-bias conductance measured by STM acquires a characteristic Fano lineshape, from which the Kondo temperature T_K is usually inferred from fittings to well-known equations.^{22,23} Such expressions, however, do not offer estimates for T_K , and rather treat it as a phenomenological fitting parameter. In fact, as we discuss below, quantitative estimates of T_K are not trivial to obtain in these systems with current theoretical approaches.

Here, we address this issue by employing a combination of complementary numerical methods to calculate the Kondo temperature and the density of states in the Kondo regime for complex magnetic molecules using state-of-the-art theories and a minimum of information from experimental data. Our approach relies on a combination of two powerful techniques: the first-principles GW method,²⁴⁻²⁶ one of the most advanced tools to describe the electronic structure of real materials; and the numerical renormalization group (NRG),²⁷ widely regarded as the most reliable numerical method to

study Kondo correlations. Our main goals are (i) to identify the relevant microscopic model and obtain realistic microscopic parameters from the GW molecular electronic structure and (ii) to describe the Kondo regime in a nonperturbative fashion with no additional assumptions on the shape of the Kondo resonance.

The strength of this merging lies on the complementarity of these techniques. On the one hand, *ab initio* methods face formidable challenges in the Kondo regime since the strongly correlated Kondo singlet state emerges at energy scales much smaller than the typical atomic or orbital energies and is beyond typical formulations of exchange and correlation effects. Furthermore, the many-body Kondo state is not well captured by perturbative approaches, which sometimes yield infrared divergencies at energy scales on the order of $k_B T_K$.³ On the other hand, NRG, which fully describes the Kondo regime, relies on quantum-impurity models to capture the microscopic low-energy features of the full system. In the case of organic complexes containing magnetic atoms, the presence of molecular states, additional degrees of freedom and charging effects further complicates the task of identifying the relevant low-energy microscopic model leading to the Kondo effect. In fact, the comparatively high Kondo temperatures (≥ 100 K) reported in STM measurements involving porphyrin compounds with a magnetic atom⁸⁻¹² indicate that extra, molecule- and surface-specific features play an active role in modifying the Kondo state. In all, such complexity has hindered attempts to *predict* Kondo temperature values from first-principles calculations although recent work in nanocontacts is most promising.²⁸

The presentation is organized as follows: in Sec. II we present GW results for the electronic structure of the molecule. Based on these results, we propose a realistic microscopic model in Sec. III, and NRG results for the Kondo temperature and density of states are presented in Sec. IV. We summarize our findings in Sec. V.

II. MANY-BODY ELECTRONIC STRUCTURE

In the present work, we study TBrPP-Co [5, 10, 15, 20-Tetrakis-(4-bromophenyl)-porphyrin-Co, stoichiometry $\text{CoBr}_4\text{N}_4\text{C}_{44}\text{H}_{24}$], which is composed by a porphyrin ring

with four bromophenyl groups at the end parts and a single cobalt atom at its center.^{9,12,29} The free-standing TBrPP-Co has S_4 symmetry. The anisotropic environment in the central cation creates a fourfold molecular field which splits the cation's $3d$ orbitals into three nondegenerate levels (with d_{3z^2-1} , $d_{x^2-y^2}$, and d_{xy} symmetries) and a degenerate pair (d_{xz} , d_{yz}). The molecule adsorbed on a Cu(111) surface undergoes a planar-saddle deformation that reduces symmetry even more and breaks the remaining degeneracy.¹² In the following, we restrict our analysis to the planar configuration and provide heuristic arguments for the observed reduction in T_K in the saddle conformation seen in experiments.

In a preliminary step, we use density-functional theory (DFT)³⁰ to determine the electronic structure of TBrPP-Co in gas phase. We use norm-conserving pseudopotentials³¹ for the interaction between valence and core electrons, including scalar relativistic effects. The exchange-correlation functional is calculated using the Perdew-Burke-Ernzerhof (PBE) parametrization.³² Calculations are done using the PARSEC code.^{33,34} We solve self-consistently the DFT equations in real space, on a regular grid with grid spacing 0.25 a.u., where 1 a.u.=0.529 Å. Electron wave functions are set to zero outside a domain enclosing the molecule. The distance between the domain boundary and any atom is at least 4 a.u. thus removing any unwanted effects arising from the scattering of electrons off the boundary. The DFT results are compatible with previous calculations on TBrPP-Co³⁵ and similar molecules.³⁶

In order to obtain accurate energies of electronic orbitals, we use the GW method.²⁴⁻²⁶ This approach is advantageous because it provides very accurate relative positions of localized d orbitals and of more extended sp orbitals.^{25,37} More specifically, most existing approximations used in DFT underestimate the value of the Coulomb gap while the GW method typically yields a better value and predicts molecular orbitals with energy ordering in better agreement with experiments.

The GW method is essentially a perturbative approach based on calculating the electron self-energy by summing only Feynman diagrams with low order in the screened Coulomb interaction W . At lowest order, the self-energy is simply $\Sigma = iG_0W$, which explains the name of the approximation. G_0 here is the Green's function of an effective noninteracting system, such as the Kohn-Sham (DFT) system. At the next level of approximation, vertex corrections are added to the previous equation: $\Sigma = iG_0W\Gamma$. We use a simplified form of the vertex, built from the DFT local density approximation. More details about the construction of the local density approximation vertex and its impact on the electronic structure of confined nanostructures can be found in Refs. 26 and 38, and references therein. After the self-energy is calculated, we diagonalize the quasiparticle eigenvalue equation

$$\left[\frac{-\nabla^2}{2m} + V_e \right] \phi_i(\mathbf{r}) + \int d\mathbf{r}' \Sigma(\mathbf{r}, \mathbf{r}', E_i) \phi_i(\mathbf{r}') = E_i \phi_i(\mathbf{r}), \quad (1)$$

where V_e is the sum of electron-ion potential (replaced with a pseudopotential in our calculations) and electrostatic poten-

tial created by electrons. Self-consistency between the Green's function and self-energy can be added by replacing G_0 with a Green's function of the real system:^{37,39,40} $\Sigma = iGW\Gamma$, and repeating the calculations of self-energy, polarizability, and Green's function until self-consistency among these quantities is found. We do not pursue full self-consistency because it is not clear how the vertex function should be updated during the process. Instead, we perform only one self-consistency cycle and assume that self-consistency is usually obtained after a small number of iterations, if the starting electronic structure is similar enough to the converged electronic structure.^{37,41} The results presented in Figs. 2 and 3 were obtained using the ϕ_i orbitals [see Eq. (1)].

Owing to the simplicity of the subsequent Anderson model and to the fact that spin transport is dominated by interactions in the vicinity of the central atom, we carry out the GW calculations assuming that electronic screening in TBrPP-Co originates predominantly from the surrounding porphyrin molecule, with very small contribution from the central cobalt atom. Following this assumption, we compute the screened Coulomb interaction W of the nonmagnetic molecule TBrPP-Ca (with calcium in the center of the porphyrin ring) and use it in the calculation of TBrPP-Co.

Several features of TBrPP-Co justify this methodology: (i) cobalt $3d$ orbitals are localized and polarize at an energy much higher than the other valence electrons in the molecule. This is a direct consequence of spatial localization of those orbitals and of small hybridization between Co $3d$ orbitals and orbitals of the TBrPP compound. (ii) Co $3d$ orbitals retain most of their identity (i.e., have a high projection on atomic Co $3d$ orbitals) even when surrounded by the nonmagnetic TBrPP structure. From that, we infer that chemical bonds between nitrogen atoms and the central atom are weak. (iii) The weight of $3d$ orbitals in the overall screening of TBrPP-Co is small as TBrPP has many more valence electrons than Co. Moreover, the properties of those electrons (energy, spatial distribution, and electric susceptibility) are very robust with respect to the type of metallic atom used, as we have checked with DFT-generalized gradient approximation (GGA) calculations for compounds of the series TBrPP- M (M =Mn, Fe, Co, Cu, Ca), which show similar electronic structure and also very similar static susceptibility. For TBrPP-Ca, we computed the screened Coulomb interaction within the time-dependent local density approximation (TDLDA),²⁶ summing 1875 virtual orbitals. The energy difference between the highest virtual orbital and the lowest-unoccupied molecular orbital (LUMO) is approximately 28 eV.

As Shirley and Martin reported,⁴² $3s$ and $3p$ orbitals correlate strongly with $3d$ orbitals. Thus, we built a pseudopotential for Co that retains the orbitals $3s$ and $3p$ in the valence shell⁴² and used this configuration in all GW calculations. In the calculations of TBrPP-Ca, we use a grid spacing of 0.35 a.u.

Figure 1 depicts the relative position of electronic orbitals of gas phase TBrPP-Co, obtained from our first-principles GW calculations. Several orbitals around the highest-occupied molecular orbital (HOMO) are strongly localized on the cobalt site and are easily identified with atomic $3d$

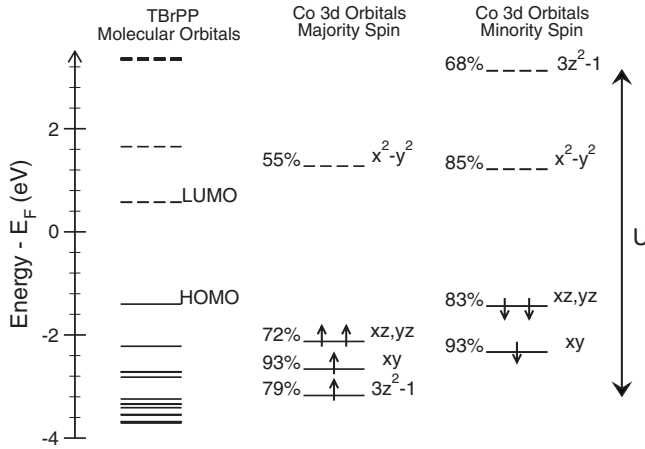


FIG. 1. Energy of electronic orbitals of TBrPP-Co in gas phase, obtained from first-principles GW calculations. The calculated Coulomb energy cost U for double occupation of the d_{3z^2-1} orbital is also indicated. Orbitals in the middle and right columns have projection on Co $3d$ atomic orbitals indicated. The “HOMO” and “LUMO” labels refer, respectively, to occupied and unoccupied orbitals in the nonmagnetic TBrPP. The Fermi energy E_F indicated is an estimate of the actual Fermi energy of adsorbed TBrPP-Co on copper (see text).

orbitals. All of them are occupied except for the $d_{x^2-y^2}$, which is completely empty, and the d_{3z^2-1} , which is populated by one unpaired electron. The z direction is perpendicular to the plane of the molecule. The intrinsically molecular orbitals (i.e., orbitals with weak $3d$ character) are nonmagnetic. The partially occupied orbital d_{3z^2-1} gives a net spin of one half, $J^2 = 3\hbar^2/4$, to the molecule. This orbital, responsible for spin magnetization, is oriented along the direction perpendicular to the plane of the porphyrin ring, giving a strong coupling with both the surface and the STM tip. These two features confirm that the d_{3z^2-1} orbital is the origin of spin-dependent transport in STM experiments.

We should emphasize the distinctions between the GW results presented in Fig. 1 and the corresponding calculation within DFT-GGA (not shown). The most significant differences between the predictions of DFT-GGA and GW results are in the energy difference between occupied molecular orbitals and unoccupied molecular orbitals. This is a manifestation of the “band-gap underestimation,” which is systematically observed when one compares these two theories. In TBrPP-Co, DFT-GGA predicts the occupied orbitals to have energies much higher than the GW estimate. As consequence, the HOMO-LUMO gap changes from 2.0 (GW) to 0.55 eV (DFT-GGA). Additionally, the value of the majority-minority splitting in the d_{3z^2-1} orbital is $U = 3.00$ eV within DFT-GGA and $U = 6.30$ eV within GW (Fig. 1).⁴³

Our calculations indicate that, although the d_{3z^2-1} orbital is localized around the central atom, it would actually penetrate deep into the surface upon deposition (see Fig. 2). This is a consequence of the strong anisotropy of the d orbital and its orientation perpendicular to the plane of the molecule. Some nonmagnetic orbitals around the Fermi energy are also extended along the z direction. In fact, Fig. 2(a) shows that the HOMO-1 (second highest occupied orbital), HOMO and

LUMO extend in the out-of-plane direction over a similar range as the d_{3z^2-1} orbital, indicating a similar penetration depth into the surface.

We quantify the extension of each orbital in the z direction by computing its accumulated density at a distance D from a plane containing the center of the molecule

$$I_i(D) = \int_A d^2\mathbf{r} \int_D^\infty dz |\phi_i(\mathbf{r}, z)|^2, \quad (2)$$

where i labels the orbital. GW results for $I_i(D)$ for the HOMO-1, HOMO, LUMO, and the d_{3z^2-1} are shown in Fig. 3. DFT-GGA results are also shown for comparison.

The fact that orbitals with comparable extent and different angular character exist is a strong indication that the high Kondo temperatures and Fano lineshapes observed in experiments^{9,12} are the result of scattering interference involving the polarized, localized orbital, and nonpolarized orbitals in the molecule.

As the molecule is adsorbed on the surface, hybridization between molecular and surface states will generally lead to charge transfer from the surface to the molecule. To verify the effect of such transfer on the levels involved in the Kondo effect, we performed DFT (PBE) calculations for the Co-porphyrin molecule on a monolayer of Cu(111). In these calculations, we also used the PARSEC code but now with periodic boundary conditions along all three spacial directions. The monolayer was modeled as an hexagonal supercell with 81 Cu atoms on the xy plane and 26 a.u. separating one monolayer from its neighboring images.

We observe that the system relaxes to a configuration where the molecule-surface hybridization is stronger for levels localized in the bromine rings, whose energies lie well below the Fermi level. Thus, the relative position of the energy levels involved in the Kondo effect (i.e., those close to the Fermi energy) remains essentially unchanged once the molecule is adsorbed. These include the cobalt-like molecular levels and the HOMO/LUMO pair depicted in Figs. 1 and 2, for which the effect of charge transfer is chiefly a uniform shift of the Fermi energy of the system (as the chemical potentials of the molecule and the surface are aligned) while the relative energy positions of these molecular states and, most importantly, the net magnetization remains unchanged.

We believe such a robustness of the magnetization arises from the relatively large separation in energy (≥ 0.5 eV) of the Cobalt $3d$ orbitals (Fig. 1). The perturbation induced by the surface potential on the cobalt atom is small in this energy scale and thus the occupation of the orbitals does not change significantly.

III. EFFECTIVE ANDERSON MODEL

Using information from GW calculations, we construct a microscopic model with realistic parameters for the system and calculate the properties in the Kondo regime using NRG. In STM experiments with the STM tip located on top of the cobalt atom, the typical width of the Kondo signal corresponds to small surface-tip bias values as compared to the characteristic spacing of electronic levels in the molecule. In

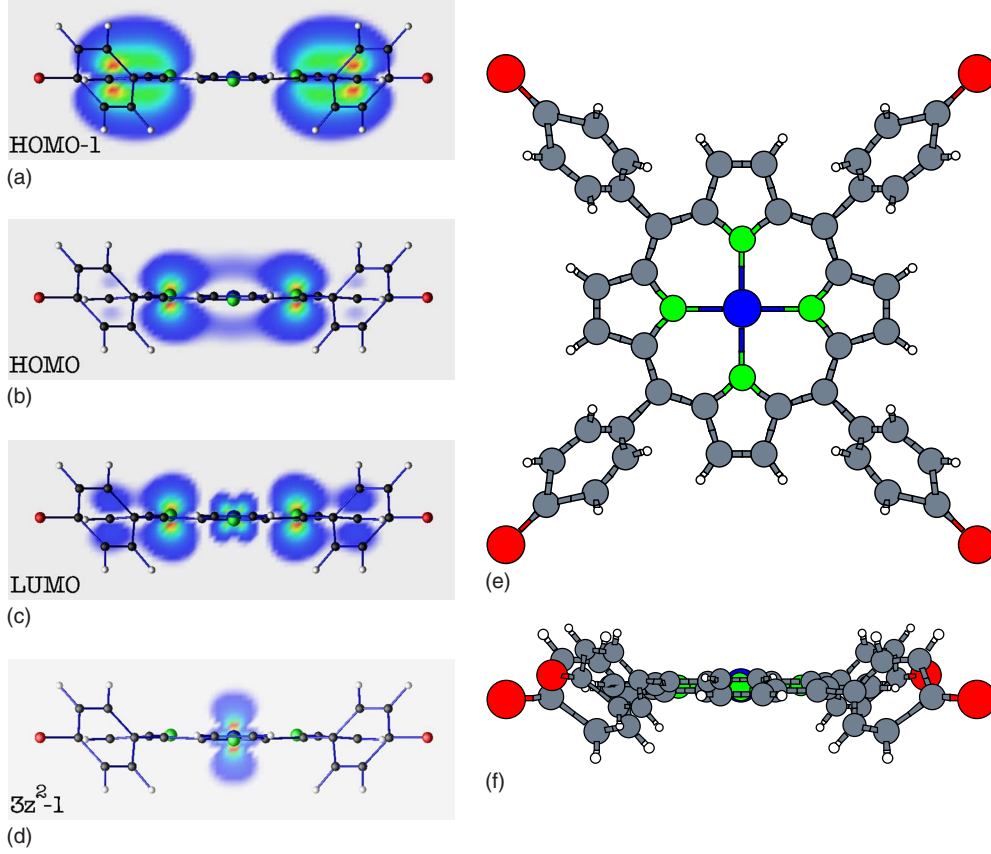


FIG. 2. (Color online) (a) Probability distribution of GW molecular orbitals HOMO-1, HOMO, LUMO, and d_{3z^2-1} on a plane perpendicular to the plane of the porphyrin ring and crossing neighbor atoms N–Co–N. Probability is highest at the center of the regions enclosed by dark “halos”. The lowest amplitude background was replaced with white and therefore the extent of the outer dark “halos” is somewhat arbitrary. The TBrPP-Co molecule is shown in front view (e) and side view (f). A single cobalt atom is coupled to four nitrogen atoms at the center of a porphyrin ring. Four bromophenyl groups are symmetrically connected to the porphyrin unit, with the bromine atoms located at the end corners.

this regime, electronic transport is dominated by elastic processes at energies close to the Fermi energy, E_F . This low-energy behavior can be captured by a model that includes both the singly occupied d_{3z^2-1} level as well as a molecular orbital M with a strong projection along the z direction at the central position and with energy closest to E_F (i.e., the HOMO in Fig. 1).⁴⁴

The Hamiltonian for such an Anderson-type model is written as

$$H = H_{\text{mol}} + H_{\text{surf}} + H_{\text{coupling}}. \quad (3)$$

The first term describes the molecular levels involved in transport. For the description of the Kondo regime, the geometry of the molecule+surface+tip configuration favors orbitals with strong z projections which are either singly occupied (giving the molecule an effective magnetic moment) or with an energy relatively close to the Fermi level (contributing to electronic transport). We thus have

$$H_{\text{mol}} = \sum_{\sigma} E_d \hat{n}_{d\sigma} + U \hat{n}_{d\uparrow} \hat{n}_{d\downarrow} + \sum_{M\sigma} E_M \hat{n}_{M\sigma} \quad (4)$$

with E_i being the GW energy of the d_{3z^2-1} orbital ($i=d$) or some molecular orbital ($i=M$), U represents the Coulomb

energy cost for double occupation in the d level, and $\hat{n}_{i\sigma}$ is the occupation number of electrons with spin σ in orbital i .

The remaining terms in Eq. (3) represent the metallic states on the surface and the molecule-surface couplings

$$H_{\text{surf}} = \sum_{\mathbf{k}\sigma} \epsilon_{\mathbf{k}} \hat{n}_{\mathbf{k}\sigma},$$

$$H_{\text{coupling}} = \sum_{\mathbf{k}} (V_{d\mathbf{k}} c_{d\sigma}^{\dagger} c_{\mathbf{k}\sigma} + \text{H.c.}) + \sum_{M,\mathbf{k}} (V_{M\mathbf{k}} c_{M\sigma}^{\dagger} c_{\mathbf{k}\sigma} + \text{H.c.}), \quad (5)$$

where the operator $c_{i\sigma}^{\dagger}$ ($c_{i\sigma}$) creates (destroys) an electron on orbital i and $V_{i\mathbf{k}} \equiv \langle \phi_i | \hat{H} | \psi_{\mathbf{k}} \rangle$ is the hybridization matrix element between orbital i and the Bloch state with vector \mathbf{k} in the metal.

The effects of the noninteracting molecular level terms ($i=M$) on the low-energy properties has been discussed in detail in Refs. 45 and 46 in the context of quantum dot systems, including the possibility of a “pseudogap Kondo effect” for $E_M = E_F$.^{45,46} In the present case, we work on a regime where $|E_M - E_F| \ll T_K$ so that the effects of the extra

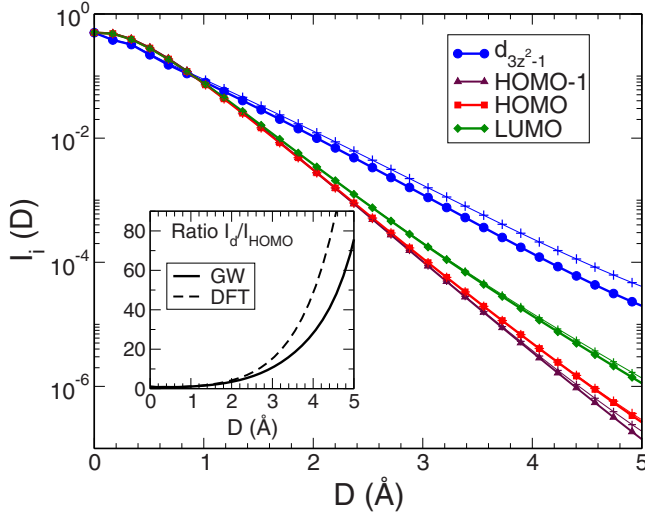


FIG. 3. (Color online) Accumulated density of orbital i (see Eq. (2)) for orbitals d_{3z^2-1} , HOMO-1, HOMO, and LUMO of TBrPP-Co in gas phase. Thick lines with filled symbols show the accumulated density calculated within the GW approximation. Thin lines with “+” signs show the corresponding accumulated densities calculated within DFT-GGA. The inset shows the ratio between integrals I_d and I_{HOMO} obtained both with GW (thick line) and DFT-GGA (dashed line). The subsequent NRG calculations were done using the GW I_d/I_{HOMO} ratio.

level is essentially to introduce corrections to the Kondo temperature as well as adding an extra resonance to the local density of states.

Model parameters directly obtained from first-principles calculations include the on-site Coulomb interaction in the d_{3z^2-1} orbital ($U=6.3$ eV) and the relative energy separation $|E_d - E_M|=1.8$ eV between the d_{3z^2-1} and the molecular orbital. The molecular-surface couplings, which give rise to the level linewidths Γ_d and Γ_M , can be estimated as a function of the central-atom-surface distance D by combining both GW results for the orbital spatial probability distributions and experimental estimates from Refs. 8, 9, and 12, as follows.

We consider two main contributions to the molecular level linewidths: an intrinsic broadening $\Gamma_{i=d,M}^{\text{GW}}$ (arising from electronic scattering processes within the molecule and obtained directly from the GW calculations) and a contribution γ_i from the hybridization with both surface and bulk metallic states [described by H_{coupling} in Eq. (5)]. The key approximation involves writing $\Gamma_i \approx \Gamma_i^{\text{GW}} + \gamma_i$,⁴⁷ where the surface contribution γ_i is directly related to the hybridization matrix elements

$$\gamma_i = -\text{Im} \lim_{\eta \rightarrow 0} \sum_{\mathbf{k}} \frac{|V_{i\mathbf{k}}|^2}{E_F - \epsilon_{\mathbf{k}} + i\eta}. \quad (6)$$

In general, γ_i will depend on the details of the overlap integrals $V_{(d,M)\mathbf{k}}$, particularly on the distance between molecule and surface. While such calculations are possible for single atoms,^{13,17} they are numerically very demanding for a molecule such as TBrPP-Co.

Instead, we take the following approach: we assume that the relevant important metallic (bulk and surface) states lead-

ing to the Kondo effect have long wavelengths so that the surface can be replaced with an electron gas occupying the half-space $z > D$. Thus, assuming the metallic states to be extended and spatially homogeneous, γ_i on each orbital can be related to the molecule-surface distance D by taking $\gamma_i \propto I_i(D)$ given by Eq. (2).

We estimate the proportionality constant by choosing Γ_d to be on the order of the d -level broadening measured in low-temperature tunneling spectroscopy for planar TBrPP-Co on Cu(111) (Ref. 9 and 12) (~ 0.3 eV) at a distance $D \sim 3$ Å, taken from Ref. 8. This sets $\Gamma_d = 0.3$ eV which, together with the calculated value for the broadening for the isolated molecule $\Gamma_d^{\text{GW}} = 0.15$ eV, gives $\gamma_d = 0.15$ eV at $D = 3$ Å. From this parameter, the ratio γ_d/γ_M for a given distance D can be obtained by calculating the ratio between the overlap integrals I_d/I_M , given by Eq. (2).

IV. KONDO PROPERTIES

The properties of the two-orbital Anderson model given in Eq. (3), consisting of an interacting d level (finite Coulomb interaction U) and a noninteracting molecular orbital coupled to a metallic channel, can be obtained with NRG. For the NRG calculations, we write the Hamiltonian given in Eq. (3) as a single-channel Anderson impurity model with an energy-dependent hybridization function^{45,46} that includes the information on the molecular orbitals.

We used a NRG discretization parameter $\Lambda = 2.5$ and kept up to 1000 states [not including SU(2) spin degeneracy] on each iteration; we use a wide-band approximation, which assumes $\Gamma_d \ll D_{\text{band}}$, where D_{band} is the bandwidth of the continuum of metallic states (which includes contributions from both surface and bulk states). To check this assumption, we performed DFT calculations for bulk Cu, which give $D_{\text{band}} \approx 10$ eV. The molecular density of states (DOS), given by $(-\pi^{-1})\text{Im}[G_d(\omega) + G_M(\omega)]$, was obtained from the interacting Green's functions $G_{d(M)}(\omega) \equiv \langle\langle c_{d(M)} : c_{d(M)}^\dagger \rangle\rangle_\omega$ calculated from NRG spectra.^{45,46} The DOS calculated in such manner contains spectral information from both “ d ” and “ M ” levels, which, based on their wave-function z extension (Fig. 3), should yield comparable contributions to the STM signal.

In the calculations, the orbital energies E_d and E_M entering the model are referenced to the Fermi energy E_F at the metallic surface. While DFT gives a crude estimate for E_F (Fig. 1), we should stress it is numerically challenging to extract a more reliable estimate for E_F from a corresponding GW calculation. Instead, we chose to treat $E_d - E_F$ as a free parameter. Thus, the surface-molecule charge transfer, identified in the DFT calculations as the mechanism controlling the relative position of the molecular orbitals to the Fermi energy, can be studied by changing E_d and E_M while keeping $E_d - E_M$ constant, which is equivalent to effectively varying the chemical potential in the molecule.

Figure 4 shows the Kondo temperature T_K as a function of $E_d - E_F$ [Fig. 4(a)] and of the central-atom-surface distance D [Fig. 4(b)], for different $E_d - E_M$ values, as shown. We find that the calculated Kondo temperatures are within the range of experimentally observed Kondo temperatures in similar systems^{8,9,12} for $D \approx 3$ Å, and charging $-0.8 \leq E_d - E_F \leq$

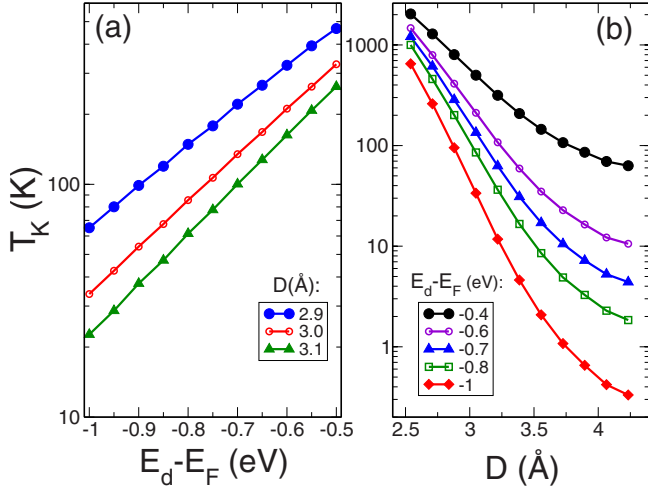


FIG. 4. (Color online) (a) Kondo temperature T_K (obtained from NRG calculations with GW-based parameters) versus (b) $E_d - E_F$ and molecule-surface distance D .

-0.6 eV (note that, in this regime, orbital M becomes the LUMO). For the value $E_d - E_F = -0.7$ eV reported in Refs. 9 and 12, we obtain $T_K \sim 140$ K for $D \approx 3$ Å, in the same range as the reported experimental results.

Overall, we obtain an exponential dependence of T_K with both D and $E_d - E_F$. Such behavior of T_K is not surprising: for $\Gamma_M \ll \Gamma_d$, the many-body Hamiltonian reduces to the usual single impurity Anderson model and one expects T_K to follow an exponential behavior³

$$T_K \sim \sqrt{\frac{U\Gamma_d}{2}} e^{-\pi|E_d - E_F||E_d - E_F + U|/2UT_d}. \quad (7)$$

The rapid decrease in T_K with D follows naturally from the dependence of the accumulated density I_d (and hence Γ_d) on D , as depicted in Fig. 2.

Interestingly, both exponential behaviors can, in a sense, compensate each other if a conformational change in the molecule decreases D and E_d at the same time, resulting in a weaker variation in T_K . In fact, this explanation is consistent with the behavior reported in Ref. 12, for which the structural change from saddle to planar conformation (reducing D) was accompanied by a slight reduction of 0.2 eV in $E_d - E_F$, leading to a moderate increase in the Kondo temperature of $\Delta T_K/T_K \sim 0.3$.

The width of the Kondo resonance in the energy-resolved DOS of the adsorbed molecule is proportional to the Kondo temperature. Experimentally, the molecule DOS can be directly probed with STM by suppressing the direct tunneling from tip to surface.⁷ We have calculated the DOS from the Green's functions for the model with NRG. Figure 5 depicts the DOS for different charge transfer ($E_M - E_F$) and distance (D) values. In all cases, the molecular LUMO resonance is prominent, as well as the Kondo peak at the Fermi energy. The E_d level is present but it is not as prominent. The width of the Kondo peak increases substantially for smaller distances and changes with charging, correlating well with the behavior of T_K in Fig. 4. Notice that the Kondo feature can

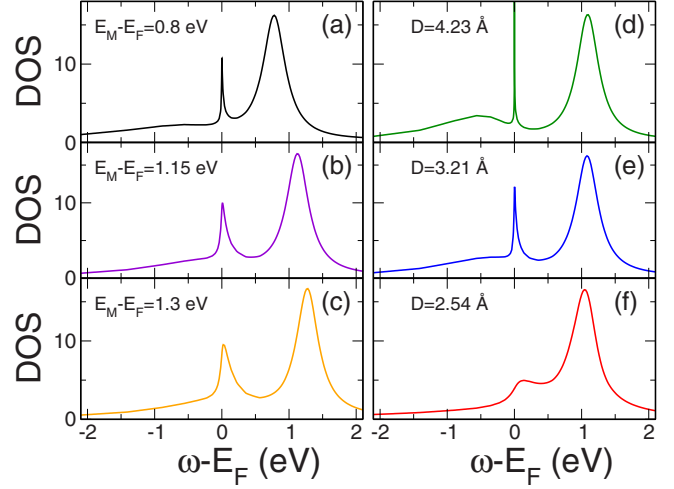


FIG. 5. (Color online) Molecular DOS system for different molecular charging [(a)–(c) $D=3$ Å] and molecule-surface distance [(d)–(f) $E_M - E_F=1.1$ eV]. A Kondo resonance at the Fermi energy and the HOMO and LUMO orbitals are shown. The width variation in the Kondo resonance ($\sim T_K$) is consistent with the results in Fig. 4.

be extremely sharp (a couple of millivolts across) for larger molecule-surface distances [Fig. 5(d)].

V. SUMMARY

In summary, we combine first-principles GW calculations with the numerical renormalization-group method and calculate Kondo temperatures of TBrPP-Co, a magnetized porphyrin compound, adsorbed on copper. This allows for a quantitative comparison with experimental results, provided that two crucial parameters are known: the separation between molecule and surface atoms, and the amount of charge transfer to or from the molecule (or, alternatively, the energy of the HOMO relative to the Fermi energy of the surface). We find that our *ab initio* treatment beyond DFT is essential, as the contribution from dynamical correlations to the molecule parameters (e.g., U , orbital energies and hybridizations) are important.

Our first-principles GW calculations indicate that there are two kinds of orbitals in the vicinity of the Fermi energy with a strong overlap with the surface: a spin-polarized d_{3z^2-1} orbital, which gives rise to the Kondo effect, and nonpolarized molecular orbitals. Both types have strong vertical projections and should dominate the observed STM conductance signal. Numerical renormalization-group calculations for a microscopic model built based on these GW results yield Kondo temperatures in good agreement to those observed in recent STM measurements.^{9,12} Additionally, the calculated DOS shows both Kondo and molecular resonances consistent with the tunneling-spectroscopy data.

We find, not unexpectedly, that the Kondo temperature and the DOS features depend strongly on the interplay between two parameters: the position of the partially occupied spin-polarized orbital with respect to the Fermi energy, which increases T_K as it approaches that energy, and the

wave function overlap between molecular orbitals and surface states, which decreases T_K as it reduces (increasing D). Most interestingly, in a regime where these two parameters compensate each other, T_K may show nonexponential behavior providing a natural explanation to recent STM measurements of T_K .

We should note the combination of numerical methods employed here is quite general and can be used to study other metallo-organic molecules. Examples are porphyrin molecules with different magnetic atoms in the center such as Fe, Cu, and Mn. Although the low-energy model extracted from the GW calculations in such cases will, in general, involve multiple orbitals and higher spin configurations, such situations can be accommodated within multiorbital extensions of the NRG method,²⁷ bringing the interesting prospect

of a comprehensive theoretical description of such strongly correlated molecular systems.

ACKNOWLEDGMENTS

We acknowledge enlightening discussions with Violeta Iancu, Saw Hla, Nancy Sandler, Kevin Ingersent, Enrique Anda, and Enrique Louis. Research was performed at the Materials Science and Technology Division, sponsored by the Division of Materials Sciences Engineering BES, U.S. DOE under contract with UT-Battelle, LLC. Computational support was provided by the National Energy Research Scientific Computing Center (NERSC), S.E.U. acknowledges support from NSF under Grants No. DMR-0336431, No. 0304314, and No. 0710581. L.G.G.V.D.S. and E.D. acknowledge support from NSF under Grant No. DMR-0706020.

*diasdasilval@ornl.gov

- ¹F. A. Reboredo and G. Galli, *J. Phys. Chem. B* **110**, 7979 (2006).
- ²M. L. Tiago, Y. Zhou, M. M. G. Alemany, Y. Saad, and J. R. Chelikowsky, *Phys. Rev. Lett.* **97**, 147201 (2006).
- ³A. C. Hewson, *The Kondo Problem to Heavy Fermions* (Cambridge University Press, Cambridge, England, 1997).
- ⁴V. Madhavan, W. Chen, T. Jamneala, M. F. Crommie, and N. S. Wingreen, *Science* **280**, 567 (1998).
- ⁵J. Li, W.-D. Schneider, R. Berndt, and B. Delley, *Phys. Rev. Lett.* **80**, 2893 (1998).
- ⁶P. Wahl, L. Diekhoner, M. A. Schneider, L. Vitali, G. Wittich, and K. Kern, *Phys. Rev. Lett.* **93**, 176603 (2004).
- ⁷A. F. Otte, M. Ternes, K. von Bergmann, S. Loth, H. Brune, C. P. Lutz, C. F. Hirjibehedin, and A. J. Heinrich, *Nat. Phys.* **4**, 847 (2008).
- ⁸A. D. Zhao, Q. X. Li, L. Chen, H. J. Xiang, W. H. Wang, S. Pan, B. Wang, X. D. Xiao, J. L. Yang, J. G. Hou, and Qingshi Zhu, *Science* **309**, 1542 (2005).
- ⁹V. Iancu, A. Deshpande, and S.-W. Hla, *Phys. Rev. Lett.* **97**, 266603 (2006).
- ¹⁰L. Gao, W. Ji, Y. B. Hu, Z. H. Cheng, Z. T. Deng, Q. Liu, N. Jiang, X. Lin, W. Guo, S. X. Du, W. A. Hofer, X. C. Xie, and H.-J. Gao, *Phys. Rev. Lett.* **99**, 106402 (2007).
- ¹¹Y.-S. Fu, S.-H. Ji, X. Chen, X.-C. Ma, R. Wu, C.-C. Wang, W.-H. Duan, X.-H. Qiu, B. Sun, P. Zhang, Jin-Feng Jia, and Qi-Kun Xue, *Phys. Rev. Lett.* **99**, 256601 (2007).
- ¹²V. Iancu, A. Deshpande, and S.-W. Hla, *Nano Lett.* **6**, 820 (2006).
- ¹³C.-Y. Lin, A. H. Castro Neto, and B. A. Jones, *Phys. Rev. B* **71**, 035417 (2005).
- ¹⁴P. Huang and E. A. Carter, *Nano Lett.* **6**, 1146 (2006).
- ¹⁵K. Leung, S. Rempe, P. Schultz, E. Sproviero, V. Batista, M. Chandross, and C. Medforth, *J. Am. Chem. Soc.* **128**, 3659 (2006).
- ¹⁶G. Chiappe and E. Louis, *Phys. Rev. Lett.* **97**, 076806 (2006).
- ¹⁷C.-Y. Lin, A. H. Castro Neto, and B. A. Jones, *Phys. Rev. Lett.* **97**, 156102 (2006).
- ¹⁸P. Huang and E. A. Carter, *Nano Lett.* **8**, 1265 (2008).
- ¹⁹J. Koseki, R. Maezono, M. Tachikawa, M. D. Towler, and R. J. Needs, *J. Chem. Phys.* **129**, 085103 (2008).
- ²⁰P. Roura-Bas, M. A. Barral, and A. M. Llois, *Phys. Rev. B* **79**, 075410 (2009).
- ²¹J. M. Aguiar-Hualde, G. Chiappe, E. Louis, E. V. Anda, and J. Simonin, *Phys. Rev. B* **79**, 155415 (2009).
- ²²O. Ujsaghy, J. Kroha, L. Szunyogh, and A. Zawadowski, *Phys. Rev. Lett.* **85**, 2557 (2000).
- ²³M. Plihal and J. W. Gadzuk, *Phys. Rev. B* **63**, 085404 (2001).
- ²⁴L. Hedin and S. Lundqvist, *Solid State Physics* (Academic, New York, 1969), Vol. 23, p. 1.
- ²⁵W. Aulbur, L. Jönsson, and J. Wilkins, *Solid State Physics* (Academic, New York, 2000), Vol. 54, p. 1.
- ²⁶M. L. Tiago and J. R. Chelikowsky, *Phys. Rev. B* **73**, 205334 (2006).
- ²⁷R. Bulla, T. A. Costi, and T. Pruschke, *Rev. Mod. Phys.* **80**, 395 (2008).
- ²⁸D. Jacob, K. Haule, and G. Kotliar, *Phys. Rev. Lett.* **103**, 016803 (2009).
- ²⁹Q. Li, S. Yamazaki, T. Eguchi, Y. Hasegawa, H. Kim, S.-J. Kahng, J. F. Jia, and Q. K. Xue, *Nanotechnology* **19**, 465707 (2008).
- ³⁰R. W. Martin, *Electronic Structure: Basic Theory and Practical Methods* (Cambridge University Press, Cambridge, UK, 2004).
- ³¹N. Troullier and J. L. Martins, *Phys. Rev. B* **43**, 1993 (1991).
- ³²J. P. Perdew, K. Burke, and M. Ernzerhof, *Phys. Rev. Lett.* **77**, 3865 (1996).
- ³³J. R. Chelikowsky, N. Troullier, K. Wu, and Y. Saad, *Phys. Rev. B* **50**, 11355 (1994).
- ³⁴<http://www.ices.utexas.edu/parsec/>
- ³⁵U. G. E. Perera, H. J. Kulik, V. Iancu, L. G. G. V. Dias da Silva, S. E. Ulloa, N. Marzari, and S.-W. Hla (unpublished).
- ³⁶M.-S. Liao and S. Scheiner, *J. Chem. Phys.* **117**, 205 (2002).
- ³⁷T. Kotani, M. van Schilfgaarde, and S. V. Faleev, *Phys. Rev. B* **76**, 165106 (2007).
- ³⁸R. DelSole, L. Reining, and R. W. Godby, *Phys. Rev. B* **49**, 8024 (1994).
- ³⁹M. L. Tiago, P. R. C. Kent, R. Q. Hood, and F. A. Reboredo, *J. Chem. Phys.* **129**, 084311 (2008).
- ⁴⁰M. S. Hybertsen and S. G. Louie, *Phys. Rev. B* **34**, 5390 (1986).

- ⁴¹M. Shishkin and G. Kresse, Phys. Rev. B **75**, 235102 (2007).
- ⁴²E. L. Shirley and R. M. Martin, Phys. Rev. B **47**, 15413 (1993).
- ⁴³As a general rule, we can use the majority-minority splitting from GW to estimate U for partially occupied d orbitals in other TBrPP- M (M =transition metal-atom) compounds. The strength of U depends crucially on the total magnetization of the molecule (TBrPP-Mn, for instance, has values of U several eVs larger than TBrPP-Co) and on the strength of the TBrPP molecular field.
- ⁴⁴The HOMO-1, HOMO-2, and HOMO-3 orbitals, although closer in energy to E_F than $3d_{z^2}$, are localized further away from the center of the molecule level, with a high amplitude on the phenyl-bromine radicals. Thus, their contribution to the STM signal with the tip placed on top of the Co atom is negligible.
- ⁴⁵L. G. G. V. Dias da Silva, N. P. Sandler, K. Ingersent, and S. E. Ulloa, Phys. Rev. Lett. **97**, 096603 (2006).
- ⁴⁶L. G. G. V. Dias da Silva, K. Ingersent, N. Sandler, and S. E. Ulloa, Phys. Rev. B **78**, 153304 (2008).
- ⁴⁷In this approximation, we are neglecting many-body contributions due to the Coulomb interactions between the electrons in orbital i entering the model (e.g., cobalt d_{3z^2-1} electrons) and the electrons in the surface. Such contributions are likely to be much smaller than the interaction effects of electrons within orbital i , which are well captured by the GW calculation in vacuum.